Progress of Thiol-Amine "Alkahest" Solutions for Thin Film Deposition

Kristopher M. Koskela, Marissa J. Strumolo, and Richard L. Brutchey*,@

Department of Chemistry, University of Southern California, Los Angeles, CA 90089, USA

Abstract: Solution deposition of thin films has garnered interest as a replacement for vacuum deposition techniques due to its scalability and lower cost. While hydrazine processing offered an alternative to vacuum deposition, its commercialization is limited due to its toxicity and explosive nature. Binary thiol-amine mixtures ("alkahests") have proven usage in the dissolution of a wide range of inexpensive, bulk solids to give inks. Intensive study of dissolution, solute speciation, and decomposition mechanisms have bridged the quality gap between hydrazine-processed and vacuum deposited thin films, but analogous studies for thiol-amine mixtures are nascent. Here, we outline recent progress made in identifying the molecular solutes from bulk solid dissolution in thiol-amine solutions. New applications and potential areas of future study are highlighted.

Solution deposition of thin films

Semiconductor thin films are used for a wide-range of technologically relevant devices, including thermoelectrics, photovoltaics, and electrocatalysts [1-4]. Traditional deposition methods, such as chemical vapor deposition and atomic layer deposition, require high vacuum, high temperatures, and specialized equipment for large-scale production [1]. In contrast, solution deposition generally utilizes lower temperatures and can be used with high-throughput techniques, such as spray coating and roll-to-roll printing, making it more cost effective and scalable [2,5,6]. A promising method for the solution deposition of semiconductor thin films is the use of molecular inks, which can produce atomically homogenous thin films with good functionality (e.g., high solar cell power conversion efficiencies) [7,8]. Molecular inks can be prepared by the dissolution of discrete molecular complexes or by the dissolution of bulk solids. Typically, discrete molecular complexes possess high solubility but are more expensive. Alternatively, the dissolution of bulk solids may be cheaper, but bulk inorganic solids often have very low solubilities in standard solvents [3,7,8].

In 2004, Mitzi and coworkers introduced hydrazine as a potent solvent that successfully co-dissolved several binary metal chalcogenides in the presence of chalcogen to produce inks that led to highly efficient solution-deposited solar cells [5]. While this system is effective, hydrazine is toxic and explosive, which limit its scalability [5,9]. Moreover, the dissolution of bulk materials in hydrazine has been limited to metal chalcogenides.

More recently, alternate solvent systems have been explored, including a binary thiol-amine mixture coined the "alkahest" introduced by Brutchey and coworkers in 2013 [10]. The alkahest is less toxic than hydrazine yet possesses high solvent power. Over 100 bulk solids, including metal chalcogenides, metal oxides, and zero-valent metals, have been dissolved with this system at room temperature and ambient pressure with solubilities of up to 30-35 wt% (as compared to 40-45 wt% for hydrazine-based inks, with respect to metal precursor dissolved) (Figure 1, Key figure) (Figure 2A) [2,5,9,11-13]. Dissolution using the alkahest is not only energetically favorable, but kinetically favorable as well. For example, Ma *et al.* were able to dissolve bulk Cu_2S in an alkahest mixture in a matter of minutes, whereas analogous dissolution in hydrazine took several days [14,15]. The alkahest generally consists of short chain thiols and primary amines, both of which are sufficiently volatile to produce homogenous thin films of the desired metal chalcogenide upon solution deposition and mild annealing (270–350 °C) [2,10,16]. Alternatively, once molecular solutes are produced by the alkahest, they can be isolated by precipitation or by evaporating the excess solvent and then re-dissolved in more conventional organic solvents for solution processing, such as DMSO, DMF, or acetonitrile [17,18]. Thin films deposited by the alkahest have been used for a variety of applications, such as electrocatalysts (Figure 2B,C) [19-23], solar cells (Figure 2D,E) [24,25], and thermoelectrics (Figure 2F,G) [26,27] with performances comparable to hydrazine fabricated devices. For example, the champion power conversion efficiencies for alkahest-processed $Cu(In,Ga)(S,Se)_2$ (CIGSSe) and $Cu_2ZnSnSe_4$ (CZTSSe) solar cells are 16.4% and 12.5%, respectively [24,25]. The champion hydrazine processed device efficiencies are 18.1% and 12.6%, respectively [28,29]. The alkahest has also been used to fabricate devices for other applications, such as photodetectors [30], wearable devices [31], and neuromorphic devices [32].

As highlighted above, the alkahest solvent system has shown remarkable solvent power for a wide range of bulk solids to solution deposit thin films for functional devices. To drive device functionality and efficiency even higher, careful consideration of the identity and decomposition properties of the resulting molecular solutes is needed to optimize thin film deposition. With a fundamental understanding of the mechanisms of dissolution and the resulting molecular species between different types of precursors (e.g., metals, metal chalcogenides, metal salts, etc.), future studies can provide insight into decomposition mechanisms with alkahest solvent systems from well-characterized molecular systems. The information garnered from these types of studies will lead to further tailoring of ink compositions with possibilities of isolating and redispersing molecular species in more polar/weakly coordinating solvents or purifying the solutes for higher quality material deposition or tailored thermal decomposition. For high efficiency devices, the number of impurities in the final materials must be limited for the commercialization of these solvent systems.

While hydrazine has several issues with its scalability as a solvent, the insights gained from this literature should not be overlooked. Metal chalcogenide devices processed from hydrazine still represent the state-of-the-art for most solution processed metal chalcogenide materials. This is due in large part to the extensive study of the mechanisms of dissolution, identities of the molecular solutes, as well as the molecular condensation and decomposition mechanisms for thin film formation [33-37]; for example, the methodologies garnered in these studies have pushed hydrazine processed CIGSSe solar cells beyond 18% power conversion efficiency [28]. While in-depth investigation into hydrazine processing has narrowed the gap between vacuum- and solution-processed devices, these types of studies are not as prevalent for alkahest systems. A review of bulk solid dissolution highlighting the resulting molecular solutes and their dissolution mechanisms is lacking. Herein, we will focus on the recent insights gained from bulk solid dissolution in alkahest systems and how these results have improved material deposition processes and motivated new applications. We will first review the current understanding of metal, metal chalcogenide, and metal salt dissolution in alkahest systems along with their resulting molecular solutes, and how fundamental understanding of dissolution can further improve device fabrication processes and efficiencies. We will then review how this knowledge has driven new applications, such as using the alkahest to engineer nanocrystal surfaces [38-40]. Finally, we will highlight the

open questions on the fundamental understanding of dissolution and decomposition mechanisms for alkahest systems and how this knowledge can lead to improved device fabrication and novel applications.

Bulk metal chalcogenide dissolution

The first report of metal chalcogenide dissolution with an alkahest solvent system came from Webber *et al.* in 2013, where nine bulk V_2VI_3 (As_2Ch_3, Sb_2Ch_3, Bi_2Ch_3, where *Ch* = S, Se, Te) chalcogenides were dissolved in a 1:10 (vol/vol) mixture of 1,2-ethanedithiol (EDT) and ethylenediamine (en) at room temperature and ambient pressure [10]. Several of the materials were dissolved within minutes. Initial attempts were made to understand alkahest dissolution through several control experiments. Besides the case of As_2S_3, which is known to dissolve in neat amines [41], the dissolution of all other V_2VI_3 chalcogenides will not proceed without thiol. It was concluded that the maximum solvent power was reached using 1,2-chelating dithiols and 1,2-chelating diamines, but mixtures of monothiols and monoamines also showed appreciable solvent power for metal chalcogenides [10]. Adding EDT to en (1:10 vol/vol) resulted in a ~15,000× increase in electrolytic conductivity through the formation of ammonium thiolates in solution [10]. To be a true molecular solution, the inks must be free of particles. Dynamic light scattering (DLS) can be used to elucidate the solvodynamic size of species in solution and can confirm when inks are fully dissolved molecular solutions. In the case of these nine bulk V_2VI_3 chalcogenides, those solutions tested (Sb_2Se_3 and Bi_2S_3) gave molecule solutes after full dissolution [10]. In the case of the Sb_2Te_3 dissolution, a polymeric Sb-Te species (>10 nm in diameter) rather than a molecular species was observed by DLS, which required the use of superhydride to fully reduce the species into a molecular solution that was processable for flexible devices (Figure 3) [42].

The first attempt to identify the resulting molecular solutes in an alkahest solvent system came from Buckley *et al.* who probed the identity of molecular stibanates from the dissolution of bulk Sb_2S_3 in mercaptoethanol (ME) and en (1:40 vol/vol) [38]. By using negative ion mode electrospray ionization mass spectrometry (ESI-MS), a mixture of four different mono- or binuclear stibanate species were identified with anionic ME ligands (Figure 3A). Inductively-coupled plasma atomic emission spectroscopy (ICP-AES) analysis of the dried ink found excess C and N that were attributed to en, with a broad ν(N–H) FT-IR stretch at 3300 cm^{-1} suggesting

that protonated en acts as a counter cation to the stibanates. To confidently identify the molecular species, careful consideration of previously reported metal-thiolate species is helpful. For example, the ion cluster assigned to $[(SC_2H_4O)Sb(SC_2H_4O)]^-$ is analogous to the molecular stibanate produced from the reaction of $Sb(O\textit{i}Pr)_3$ and ME, which yields the neutral trigonal pyramidal complex $(SC_2H_4O)Sb(SC_2H_4OH)$, where one ME ligand forms a five-membered, dianionic chelate ring and the other ME ligand binds unidentate through a thiolate [43]; indeed, there is excellent agreement between the ν(S–C), ν(C–O), and ν(Sb–OC) FT-IR bands of this complex and the observed $[(SC_2H_4O)Sb(SC_2H_4O)]^-$.

In the case of bulk Sb_2Te_3 dissolution in EDT and en (1:10 vol/vol), molecular products were precipitated with the addition of acetonitrile after reduction with superhydride (Figure 3B,E); the resulting molecular solute possessed an Sb:Te ratio of ~2:7 by energy-dispersive X-ray spectroscopy (EDS) [42]. Based on the elemental composition, the authors speculate that one possible form of this solute could be the previously reported $Sb_2Te_7^{4-}$ binuclear cluster synthesized in hydrazine [44]. This cluster was further treated with tri-*n*-octylphosphine (TOP) to abstract excess Te as TOP=Te, with the resulting antimony complex being soluble in polar solvents. This isolated purified molecular cluster led to dense, specularly reflective thin films that were processable on flexible polyimide substrates (Figure 3D,E), whereas the polymeric Sb-Te products prior to superhydride reductive gave poor film quality (Figure 3C) [42]. Similarly, for bulk Ag_2S dissolution in EDT and en (1:10 vol/vol), the resulting solutes change from being Ag-rich (with a Ag:S ratio of 2:1) to Ag-poor (with a Ag:S ratio of 2:3) after precipitation with acetonitrile. The exclusion of the unidentified Ag-rich solutes led to greatly improved film morphologies [31]. Additional studies on the exact mechanism of metal chalcogenide dissolution are warranted to possibly direct the formation of various advantageous molecular solute(s) and further optimize film deposition based on this information.

Bulk metal dissolution

Bulk metal dissolution from alkahest mixtures was first reported by Zhao *et al.*, in which bulk Cu and In powders were dissolved in EDT and en, whereas Ga dissolution required the addition of bulk Se for full dissolution [45]. A subsequent study by Zhang *et al.* reported a wider elemental range of bulk metal dissolution (i.e., Cu, In, Sn, and Zn) from a binary mixture of EDT and

butylamine (BA) or hexylamine (HA), in which binary metal chalcogenides were recovered using EDT as the only sulfur source and added chalcogen was not needed for dissolution [46]. To better understand the mechanism of dissolution with alkahest mixtures for zero-valent metals, Agrawal and coworkers attempted to isolate and identify the molecular solutes in Cu and In dissolved in mixtures of EDT and HA (1:10 vol/vol) [18]. Using these isolated species, they redispersed the solutes in DMSO for more benign solution deposition and device fabrication [18]. Both resulting Cu- and In-thiolates were isolated by evaporating the fully dissolved EDT-HA solutions (e.g., Figure 4A). The isolated species were analyzed using ESI-MS, X-ray absorption spectroscopy (XAS), and solution NMR spectroscopy. The isolated In-thiolates were found to be in the In^{3+} oxidation state with average bond distances matching well with In–S bonds and EXAFS In *K*-edge showing a local coordination number of four [18]. Coupled with ESI-MS, it was concluded that the most plausible molecular solute structure was $[In(S_2C_2H_4)_2]^-$. ^1H, ^{13}C, and 2D coupled ^1H-^{13}C NMR spectroscopy corroborated the identity of the molecular species in solution as bis(1,2-ethanedithiolate)indium(III). It has been previously reported that In-dithiolate complexes decompose to In_2S_3 whereas In-monothiolates afford InS [47]. In the case of Cu dissolution, the identification of the molecular species was more complex. XAS confirmed the exclusive presence of Cu^+ with a coordination number of three, and the large masses observed in ESI-MS suggests high nuclearity Cu-thiolate clusters with 2-8 Cu atoms [18]. As previously reported in unrelated studies on Cu-thiolate clusters, several possible geometries and structures are possible [48-50] and without direct single-crystal XRD data, the exact identity of the Cu-thiolates in amine-thiol mixtures is still unresolved. Moreover, a mechanism for In metal dissolution was proposed from gaseous product analysis, where the exothermic, oxidative dissolution of zero-valent In is driven by irreversible H_2 gas evolution (Figure 4B) [18].

For the dissolution of bulk metals, redox reactions with elemental chalcogens are typically needed for processes akin to surface tarnishing. In the early 1990s, Rauchfuss *et al.* explored the dissolution of bulk metals through an oxidative dissolution process [51-54]. Bulk Cu metal was dissolved in the presence of sulfur with the assistance of donor solvents yielding metal complexes with donor solvent and polysulfide ligands [51]. This work was expanded to several other metals (i.e., Fe, Mg, Mn, Ni and Zn) with various donor solvents (*N*-methylimidazole (MeIm), pyridine (py), tetramethylethylenediamine (TMEDA), 4-(dimethylamino)pyridine) [52,53]. It was shown

that in the case of Zn dissolution, the resulting $Zn(TMEDA)S_6$ molecular complex can be decomposed to yield cubic ZnS [54]. The dissolution of metals with sulfur and donor solvents proceeds through oxidation of the metal by the chalcogen with the strong donor-solvent interaction stabilizing the resulting molecular complex [51-53]. This chemistry was recently revisited by Wang and co-workers for the dissolution of bulk elemental Sn and Pb, where molecular dichalcogenides serve the same role as elemental chalcogens [55,56]. For example, diphenyl diselenide oxidizes both metallic Pb and Sn to give discrete Pb^{2+} and Sn^{2+} thiolate complexes, suggesting an oxidative addition reaction analogous to the mechanism proposed by Rauchfuss [55,56]. In the case of Pb dissolution, the molecular solute was isolated and analyzed by single crystal XRD that gives confirmation of a four-coordinate geometry about Pb with two selenolate ligands and two donor solvent ligands (i.e., $Pb(L)_2(SePh)_2$, where L = py, ½ en) [56]. The isolated Pb species are structurally similar to previously reported four-coordinate $(py)_2Pb(SeC_5F_5)_2$ [57] and $Pb(SeCH_2CH_2NMe_2)_2$ [58] complexes. These molecular solutes derived from Pb dissolution can be thermally decomposed to give PbSe, PbTe, and $PbSe_xTe_{1-x}$ when using diphenyl diselenide, ditelluride, or a combination of the two, respectively [55]. Along the same lines, SnSe and SnTe phases can be returned when diphenyl diselenide or ditelluride are used, respectively, to dissolve Sn metal in the presence of en, py, DMSO, or butylamine (BA) [55]. These examples suggest that zero-valent metal dissolution with thiol-amine solutions may be occurring through oxidative dissolution from the presence of adventitious disulfides, which are commonly found in thiols as oxidation products.

Metal salt dissolution

While metal chalcogenide and zero-valent metal dissolution have been studied more extensively, alkahest solutions have also been shown to dissolve a wide range of metal salts (e.g., metal acetates, acetylacetonates, halides) that return metal chalcogenide materials upon thermal annealing [59-61]. Murria *et al.* identified the speciation of molecular solutes from the dissolution of both CuCl and $CuCl_2$ in 1-propanthiol (PT) and BA solutions (1:1 mol/mol) using ESI high-resolution tandem mass spectrometry, synchrotron XAS, and Raman spectroscopy [62]. When dissolving CuCl and $CuCl_2$ in PT and BA, almost identical MS spectra were observed that suggest a mixture of various Cu-thiolate and chloride complexes that give the same colored solutions (Figure 4C,D). XAS suggested the exclusive presence of Cu^+ in solution, even for the dissolution of $CuCl_2$ [62]. While

no Cu-amine complexes were found by ESI, various sized butylammonium chloride adducts ($[C_4H_9NH_3^+]_n[Cl^-]_{n+1}$) were observed as by-products [62]. The proposed Cu-thiolate, chloride, and mixed thiolate chloride species were corroborated with quantum chemical calculations and are similar to previously calculated Cu-thiolate structures [63,64]. The observation of Cu^{2+} reduction to Cu^+ has also been observed in other alkahest processed chalcogenide materials where Cu^{2+} precursors are reduced in the final annealed material as evidenced by high-resolution XPS [11]. These findings are in agreement with previous reports that suggest Cu^{2+} reduces to Cu^+ in the presence of thiols, forming disulfides [65,66]; Cu(I) disulfide complexes are thermodynamically favored over Cu(II) μ-thiolates [67]. When these solutions were annealed to 80 °C to generate thin films, the only crystalline products detected were *n*-butylammonium chloride salts [62]. While amorphous Cu-S species were detected by Raman at 80 °C with the addition of elemental sulfur, no crystalline products were detected even when the thin films were annealed to 350 °C with or without added sulfur [62]. The authors posit that chloride impurities, observed in the molecular solutes, are inhibiting crystallization of copper sulfide phases. The use of chloride salts has also led to complications in the fabrication of CIGSSe solar cells [60]. When using $GaCl_3$ as the Ga source, or a combination of $InCl_3$ and CuCl salts with $Ga(acac)_3$, $GaCl_3$ was always found in the precursor ink [60]. Upon annealing these inks, the low volatilization temperature of $GaCl_3$ led to significant Ga loss in the final films, which was only negated by severely increasing the amount of Ga in the precursor ink or simply by using non-chloride metal precursor salts. While a wide variety of precursors have been dissolved in thiol-amine solutions, and several molecular solutes have been identified or postulated, direct comparisons between a single metal with analogous bulk solids is lacking. These types of studies can be beneficial for understanding element-specific dissolution and coordination chemistry in these solvent systems, and for subsequent thin film optimization (Box 1).

Box 1. Comparing bulk Sn, SnO, SnS, and SnSe dissolution

To identify the molecular solutes of the same metal using different bulk solid precursors, Buckley *et al.* dissolved Sn, SnO, and SnS in a mixture of EDT and en (1:10 vol/vol) to give identically colored solutions free of scattering (Figure IA) [75]. Using solution ^{119}Sn NMR, a single and identical resonance at δ_{119Sn} = 217 ppm was observed for each precursor solution, suggesting a single molecular solute that lacks any $J_{Sn\text{-}Sn}$ coupling (Figure IB) [75]. This chemical shift is indicative of four-coordinate Sn in a sulfur environment, as ^{119}Sn NMR is extremely sensitive to coordination environment [75-78]. Several control experiments were performed to confidently identify the molecular solute. For example, the independently prepared, neutral $(EDT)_2Sn(IV)$ complex exhibits a chemical shift of δ_{119Sn} = -263 ppm in the presence of en; this chemical shift window is indicative of six-coordinate species. Indeed, negative ion mode ESI-MS suggests en chelation to Sn with the main ion cluster corresponding to $[Sn(EDT)_2en]^-$. As such, this suggests the molecular solute is a four-coordinate $[(EDT)_2Sn(II)]^{2-}$ species (Figure IC), which was corroborated by a DFT calculation of the gas-phase ^{119}Sn NMR chemical shift. When these inks were annealed, all three returned crystalline and phase-pure SnS with identical optical band gaps [75].

When comparing Sn containing molecular solutes in alkahest solutions with those identified in hydrazine dissolution, several similarities are observed. The well-defined structures of Sn(IV) thiostannates (i.e., $[Sn_2S_6]^{4-}$, $[Sn_4Se_6]^{4-}$, $[Sn_4S_{10}]^{4-}$, $[Sn_4Se_{10}]^{4-}$) found in hydrazine provide characteristic vibrational and absorption spectroscopic handles [5,13,34,79-81]. In a recent study by Heo *et al.*, compositionally phase-impure thin films of Sn(S,Se) were obtained from the decomposition of inks derived from bulk SnSe dissolved in EDT and en (1:10 vol/vol) [17]. A purification step was performed whereby acetonitrile was used to precipitate solute species, which were identified as $[Sn_4Se_6]^{4-}$ and $[Sn_4Se_{10}]^{4-}$ using Raman and UV-vis spectroscopies. By using these isolated solutes and redispersing them in en, highly textured, mirror-like thin films of phase-pure SnSe were fabricated after annealing to 400 °C [17].

Film impurities from alkahest method

Minimizing impurities and defects will lead to higher quality thin film fabrication, ultimately opening the door to commercially competitive devices. While it is known that layers fabricated

from nanocrystal inks leave large carbonaceous impurities from the decomposition of long chain aliphatic ligands, alkahest inks can reduce carbon impurities. It has been seen that carbon impurities ultimately affect grain size and device performance (i.e., in CIGSSe solar cells); therefore, it is important to minimize the amount of carbon in the final films [45,68]. In an early study, the decomposition of an alkahest ink consisting of dissolved In, Ga, and Se in EDT and en led to trace carbon impurities that restricted the growth of large grain CIGSe films [45]. More recently, annealing strategies utilizing rapid thermal annealing (RTP) have been adapted to promote large grain CIGSe formation throughout the entire absorber layer using alkahest inks for deposition [68,69]. It has been suggested in a recent study by Deshmukh *et al.* that their CIGSe inks prepared by the alkahest contain no carbon impurities upon device fabrication [70].

Another possible limitation of alkahest inks is the incorporation of sulfur, from thiol decomposition, during the crystallization of selenide and telluride thin films. Webber *et al.* reported the incorporation of ~2 at% S upon decomposition and crystallization of a Sb_2Se_3 ink at 350 °C [10]. In the case of Sb_2Se_3, incorporation of sulfide impurities can be circumvented by using bulk elemental Sb and Se in inks containing EDT and en, where no sulfur impurities were detected by EDS upon recovery of the thin film [71]. While design strategies to avoid impurities in the final materials can be gleaned from these results, decomposition mechanisms from well-characterized molecular solutes are needed to obtain a better understanding of these effects. In the case of CIGSSe inks in thiol-amine solvent mixtures, the amount of sulfur in the final thin film can be severely limited upon high temperature selenization [60,68].

New applications of alkahest solutions

Drawing inspiration from the hydrazine dissolution literature, the molecular solutes in alkahest solutions can also facilitate phase-transfer ligand exchange on colloidal nanocrystals and subsequently act as a molecular glue or solder between the nanocrystals in thin films [38-40]. The first application of nanocrystal ligand exchange using alkahest solutions came from Buckley *et al.*, where molecular stibanates (*vide supra*), in addition to dissolved As_2S_3, As_2Se_3, Sb_2Se_3, SnS, and ZnS species, were used to replace bulky organic ligands on the surface of CdSe, CdS/CdSe core/shell, and Pt nanocrystals (Figure 5A,B) [38]. Absorption spectra of the ligand-exchanged CdSe and CdS/CdSe core/shell nanocrystals showed little-to-no spectral changes in the position of

the exciton peak, indicating the particles are not etched (Figure 5C). A >25-fold increase in the electrochemical photocurrent density was measured when installing the molecular stibinates on CdSe nanocrystals because of better nanocrystal-nanocrystal coupling (Figure 5D). This methodology was extended to colloidal PbS nanocrystals by Ibáñez *et al.*, where elemental S and Te were separately dissolved in mixtures of EDT and en and used to exchange the oleate-capped surfaces of PbS nanocrystals [39]. It was shown that after thermal annealing, PbS nanocrystals treated with dissolved sulfur complexes increased the carrier concentration in nanocrystal-derived dense pellets by over an order of magnitude. Conversely, when PbS nanocrystals were treated with dissolved Te complexes, carrier concentrations decreased by an order of magnitude. Such an approach could therefore be used to tune transport in nanocrystal solids for applications in thermoelectrics and optoelectronics. Ibáñez *et al.* expanded on this strategy by installing alkahest-dissolved elemental Cd and Se onto the surfaces of SnTe nanocrystals [40]. It was proposed that the solution of Cd and Se dissolved in EDT and en consisted of $(Cd_2Se_3)_n^{2n-}$ or $CdSe_2^{2-}$ chalcogenidocadmates by extension to the analogous solutes in hydrazine solutions [40,72,73]; however, these species were not characterized. When these materials were pressed and annealed, CdSe surface alloying led to an increased Seebeck coefficient and power factor that also yielded nanoinclusions of CdSe in the SnTe matrix. Resulting band engineering (i.e., wider band gap, diminished energy separation between light-hole band and heavy hole-band) led to a higher *ZT* than analogous thiocyanate-treated SCN-SnTe nanocrystals (Figure 5E) [40]. Surface alloying with Cd in the SnTe nanocrystals was confirmed through annular dark field (ADF) scanning transmission electron microscopy (STEM) that showed amorphous coverage of Cd on SnTe nanocrystals (Figure 5F). These types of studies using alkahest-derived solutes for nanocrystal surface engineering are gaining traction; this methodology can be used to replace hydrazine elsewhere, such as using In-chalcogenidometallates (such as $In_2Se_4^{2-}$ or others) to ligand exchange CdSe nanocrystals [74].

Concluding remarks

In a short amount of time, binary combinations of thiol and amines have become an incredibly useful solvent mixture for the facile dissolution of a wide range of bulk solids that are generally thought to be insoluble under standard conditions. This has enabled a large palette of inks to be developed for the solution deposition of metal chalcogenide thin films with controllable

compositions and functionality. To further improve the effectiveness of alkahest chemistry for the solution deposition of thin films, careful consideration must be given to the identity of dissolved molecular solutes and their subsequent effect on the resulting material properties in order to close the quality gap with hydrazine-processed thin films. Future studies should be devoted to developing a chemical understanding of the dissolution mechanisms with different types of starting solids, such as bulk metal chalcogenides and oxides, and more focused efforts on the direct characterization of resulting solutes (e.g., by single crystal X-ray diffraction rather than indirect MS methods where ionization may affect the solute identity) and potential deleterious byproducts. With structurally well-defined molecular solutes in hand, studying their subsequent decomposition to metal chalcogenides will enable further optimization of thin film deposition (see Outstanding Questions). To keep pace with rapidly evolving solution deposition techniques, findings from these types of studies could ultimately lead to state-of-the-art materials or devices with competitive functionality.

Acknowledgements

R.L.B. acknowledges support from the National Science Foundation under DMR-1904719.

Declaration of interests

Authors declare no competing interests.

References

1. Matthews, P. D. *et al.* (2017) Shining a light on transition metal chalcogenides for sustainable photovoltaics. *Chem. Sci*. 8, 4177-4187
2. McCarthy, C. L. *et al.* (2017) Solution processing of chalcogenide materials using thiol–amine ‘‘alkahest’’ solvent systems. *Chem. Commun.* 53, 4888-4902
3. Jo, S. *et al.* (2019) Ink processing for thermoelectric materials and power-generating devices. *Adv. Mater.* 31, 1804930
4. McCarthy, C. L. *et al.* (2018) Preparation of electrocatalysts using a thiol–amine solution processing method. *Dalton Trans.* 47, 5137-5143
5. Mitzi, D. B. *et al.* (2004) High-mobility ultrathin semiconducting films prepared by spin coating. *Nature* 428, 299-303

6. Suresh, S. *et al.* (2021) Present status of solution-processing routes for Cu(In,Ga)(S,Se)$_2$ solar cell absorbers. *Adv. Energy Mater.* 11, 2003743
7. Habas, S. E. *et al.* (2010) Low-cost inorganic solar cells: from ink to printed device. *Chem. Rev.* 110, 6571-6594
8. Clark, J. A. *et al.* (2019) Complexation chemistry in *N,N*-dimethylformamide-based Molecular inks for chalcogenide semiconductors and photovoltaic devices. *J. Am. Chem. Soc.* 141, 298-308
9. Mitzi, D. B. (2008) Solution processing of chalcogenide semiconductors via dimensional reduction, *Solution Processing of Inorganic Materials* (Mitzi, D. B.), pp.77-108, John Wiley & Sons
10. Webber, D. H. *et al.* (2013) Alkahest for V_2VI_3 chalcogenides: dissolution of nine bulk semiconductors in a diamine-dithiol solvent mixture. *J. Am. Chem. Soc.* 135, 15722-15725
11. Koskela, K. M. *et al.* (2020) Solution deposition of a bournonite $CuPbSbS_3$ semiconductor thin film from the dissolution of bulk materials with a thiol-amine solvent mixture. *J. Am. Chem. Soc.* 142, 6173-6179
12. McCarthy, C. L. *et al.* (2015) Solution-phase conversion of bulk metal oxides to metal chalcogenides using a simple-thiol solvent mixture. *Angew. Chem., Int. Ed.* 54, 8378-8381
13. Mitzi, D. B. (2005) Synthesis, structure, and thermal properties of soluble hydrazinium germanium(IV) and tin(IV) selenide salts. *Inorg. Chem.* 44, 3755-3761
14. Ma, Y. *et al.* (2016) Thermoelectric properties of copper chalcogenide alloys deposited via the solution-phase using a thiol-amine solvent mixture. *RSC Adv.* 6, 99905-99913
15. Mitzi, D. B. *et al.* (2008) A high-efficiency solution-deposited thin-film photovoltaic device. *Adv. Mater.* 20, 3657-3662
16. Albalawneh, G. *et al.* (2020) Review-solution processing of CIGSe solar cells using simple thiol-amine solvents mixture: a review. *ECS J. Solid State Sci. Technol.* 9, 061013
17. Heo, S. H. *et al.* (2019) Composition change-driven texturing and doping in solution-processed SnSe thermoelectric thin films. *Nat. Commun.* 10, 864
18. Zhao, X. *et al.* (2019) Investigating chemistry of metal dissolution in amine-thiol mixtures and exploiting it toward benign ink formulation for metal chalcogenide thin films. *Chem. Mater.* 31, 5674-5682

19. Liu, F. *et al.* (2015) Low-temperature, solution-deposited metal chalcogenide films as highly efficient counter electrodes for sensitized solar cells. *J. Mater. Chem. A* 3, 6315-6323
20. Lui, F. *et al.* (2015) Earth-abundant Cu_2SnSe_3 thin film counter electrode for high-efficiency quantum dot-sensitized solar cells. *J. Power Sources* 292, 7-14
21. Zhao, X. *et al.* (2017) An ambient temperature, CO_2-assisted solution processing of amorphous cobalt sulfide in a thiol/amine based quasi-ionic liquid for oxygen evolution catalysis. *Chem. Commun.* 53, 9418-9421
22. McCarthy, C. L. *et al.* (2016) Method for the solution deposition of phase-pure $CoSe_2$ as an efficient hydrogen evolution reaction electrocatalyst. *ACS Energy Lett.* 1, 607-611
23. McCarthy, C. L. *et al.* (2017) Room temperature dissolution of bulk elemental Ni and Se for solution deposition of a $NiSe_2$ HER electrocatalyst. *Inorg. Chem.* 56, 10143-10146
24. Zhao, Y. *et al.* (2020) Controllable formation of ordered vacancy compound for high efficiency solution processed $Cu(In,Ga)Se_2$ solar cells. *Adv. Funct. Mater.* 31, 2007928
25. Zhao, Y. *et al.* (2021) Local Cu component engineering to achieve continuous carrier transport for enhanced kesterite solar cells. *ACS Appl. Mater. Interfaces* 13, 795-805
26. Lin, Z. *et al.* (2015) Cosolvent approach for solution-processable electronic thin films. *ACS Nano* 9, 4398-4405
27. Lin, Z. *et al.* (2017) A solution processable high-performance thermoelectric copper selenide thin film. *Adv. Mater.* 29, 1606662
28. Zhang, T. *et al*. (2016) High efficiency solution-processed thin-film $Cu(In,Ga)(Se,S)_2$ solar cells. *Energy Environ. Sci.* 9, 3674
29. Wang, W. *et al.* (2014) Device characteristics of CZTSSe thin-film solar cells with 12.6% efficiency. *Adv. Energy Mater.* 4, 1301465
30. Hasan, M. R. *et al.* (2016) An antimony selenide molecular ink for flexible broadband detectors. *Adv. Electron. Mater.* 2, 1600182
31. Jo, S. *et al.* (2021) Solution-processed stretchable Ag_2S semiconductor thin films for wearable self-powered nonvolatile memory. *Adv. Mater.* 33, 2100066
32. Harikesh, P. C. *et al.* (2020) Cubic $NaSbS_2$ as an ionic-electronic coupled semiconductor for switchable photovoltaic and neuromorphic device applications. *Adv. Mater.* 32, 1906976

33. Bob, B. *et al.* (2012) The development of hydrazine-processed Cu(In,Ga)(Se,S)$_2$ solar cells. *Adv. Energy Mater.* 2, 504-522
34. Nørby, P. *et al.* (2014) $(NH_4)_4Sn_2S_6 \cdot 3H_2O$: Crystal structure, thermal decomposition, and precursor for textured thin film. *Chem. Mater.* 26, 4494-4504
35. Chung, C.-H. *et al.* (2011) Identification of the molecular precursors for hydrazine solution processed $CuIn(Se,S)_2$ films and their interactions. *Chem. Mater*. 23, 964-969
36. Yang, B. *et al.* (2015) Hydrazine solution processed Sb_2S_3, Sb_2Se_3 and $Sb_2(S_{1-x}Se_x)_3$ film: molecular precursor identification, film fabrication and band gap tuning. *Sci. Rep.* 5, 10978
37. Yang, W. *et al.* (2013) Molecular solution approach to synthesize electronic quality Cu_2ZnSnS_4 thin films. *J. Am. Chem. Soc.* 135, 6915-6920
38. Buckley, J. J. *et al.* (2014) Ligand exchange of colloidal CdSe nanocrystals with stibanates derived from Sb_2S_3 dissolved in a thiol-amine mixture. *Chem. Mater.* 26, 6311-6317
39. Ibáñez, M. *et al.* (2017) Tuning *p*-type transport in bottom-up-engineered nanocrystalline Pb chalcogenides using alkali metal chalcogenides as capping ligands. *Chem. Mater.* 29, 7093-7097
40. Ibáñez, M. *et al.* (2019) Ligand-mediated band engineering in bottom-up assembled SnTe nanocomposites for thermoelectric energy conversion. *J. Am. Chem. Soc.* 141, 8025-8029
41. Slang, S. *et al.* (2015) Mechanism of the dissolution of As-S chalcogenide glass in *n*-butylamine and its influence on the structure of spin coated layers. *J. Non-Cryst Solids* 426, 125-131
42. Jo, S. *et al.* (2019) Soluble telluride-based molecular precursor for solution-processed high-performance thermoelectrics. *ACS Appl. Energy Mater.* 2, 4582-4589
43. Gupta, A. K. S. *et al.* (1990) Heterocyclic compounds containing antimony 1. Synthesis, physiochemical properties, crystal and molecular structure of 2-(β-hydroxyethylthio)1,3,2-oxathiastibolane. *Inorg. Chim. Acta* 170, 191-197
44. Kovalenko, M. V. *et al.* (2010) Semiconductor nanocrystals functionalized with antimony telluride zintl ions for nanostructured thermoelectrics. *J. Am. Chem. Soc.* 132, 6686-6695
45. Zhao, D. *et al.* (2015) Solution-deposited pure selenide CIGSe solar cells from elemental Cu, In, Ga, and Se. *J. Mat. Chem A* 3, 19263

46. Zhang, R. *et al.* (2016) Metal-metal chalcogenide molecular precursors to binary, ternary, and quaternary metal chalcogenide thin films for electronic devices. *Chem. Commun.* 52, 5007
47. Nomura, R. (1989) Thermal decomposition of butylindium thiolates and preparation of indium sulfide powders. *Appl. Organomet. Chem.* 3, 195-197
48. Pickering, I. J. *et al.* (1993) X-Ray absorption spectroscopy of cuprous-thiolate clusters in proteins and model systems. *J. Am. Chem. Soc.* 115, 9498-9505
49. Pushie, M. J. *et al.* (2012) The fictile coordination chemistry of cuprous-thiolate sites in copper chaperones. *Biochim. Biophys. Acta, Bioenerg.* 1817, 938-947
50. Rao, C. P. *et al.* (1986) Synthesis and structural systematics of ethane-1,2-dithiolato complexes. *Inorg. Chem.* 25, 428-439
51. Ramli, E. *et al.* (1990) Inception of copper polysulfide clusters in the reaction of copper and sulfur in donor solvents: polysulfide complexes as the link between molecular and nonmolecular metal sulfides. *J. Am. Chem. Soc.* 112, 4043-4044
52. Dev, S. *et al.* (1990) Direct approaches to zinc polychalcogenide chemistry: ZnS_6(*N*-MeIm)$_2$ and $ZnSe_4$(*N*-MeIm)$_2$. *J. Am. Chem. Soc.* 112, 6385-6386
53. Dev, S. *et al.* (1991) Synthesis and structure of [M(*N*-methylimidazole)$_6$]S_8 (M = Mn, Fe, Ni, Mg). Polysulfide salts prepared by the reaction *N*-methylimidazole + metal powder + sulfur. *Inorg. Chem.* 30, 2514
54. Verma, A. K. *et al.* (1995) Donor solvent mediated reactions of elemental zinc and sulfur, *sans* explosion. *Inorg. Chem.* 34, 3072-3078
55. Wang, Z. *et al.* (2018) Precursors for PbTe, PbSe, SnTe, and SnSe synthesized using diphenyl dichalcogenides. *Chem. Comm.* 54, 9055
56. Vartak, P. B. *et al.* (2020) Solution and solid-state characterization of PbSe precursors. *ACS Omega* 5, 1949-1955
57. Holligan, K. *et al.* (2015) Copper, indium, tin, and lead complexes with fluorinated selenolate ligands: precursors to MSe_x. *Inorg. Chem.* 54, 8896-8904
58. Kedernath, G. *et al.* (2009) β-functionalized ethylchalcogenolate complexes of lead (II): synthesis, structures and their conversion into lead chalcogenide nanoparticles. *Polyhedron* 28, 2749-2753

59. Zhang, R. *et al.* (2015) A versatile solution route to efficient $Cu_2ZnSn(S,Se)_4$ thin-film solar cells. *Chem. Mater.* 27, 2114-2120
60. Zhao, X. *et al.* (2016) Solution-processed sulfur depleted Cu(In, Ga)Se_2 solar cells synthesized from a monoamine-dithiol solvent mixture. *J. Mater. Chem. A* 4, 7390
61. Wu. W.-Y. *et al.* (2019) Thermochromism from ultrathin colloidal Sb_2Se_3 nanowires undergoing reversible growth and dissolution in an amine-thiol mixture. *Adv. Mater.* 31, 1806164
62. Murria. P. *et al.* (2017) Speciation of CuCl and $CuCl_2$ thiol-amine solutions and characterization of resulting films: implications for semiconductor device fabrication. *Inorg. Chem.* 56, 14396-14407
63. Howell, J. A. S. (2006) Structure and bonding in cyclic thiolate complexes of copper, silver and gold. *Polyhedron* 25, 2993-3005
64. Kacprzak, K. A. *et al.* (2010) Theoretical characterization of cyclic thiolated copper, silver, and gold clusters. *J. Phys. Chem. C* 114, 13571-13576
65. Hellinga, H. W. (1990) Construction of a blue copper analogue through iterative rational protein design cycles demonstrates principles of molecular recognition in metal center formation. *J. Am. Chem. Soc.* 120, 10055-10066
66. Smith, R. C. *et. al.* (1994) Oxidation of thiols by copper(II). *Phosphorus, Sulfur Silicon Relat. Elem.* 90, 147-154
67. Ording-Wenker, E. C. M. *et al.* (2014) Thermodynamics of the Cu^{II} μ-Thiolate and Cu^{I} disulfide equilibrium: A combined experimental and theoretical study. *Inorg. Chem.* 53, 8494-8504
68. Arnou, P. *et al.* (2016) Hydrazine-free solution-deposited CuIn$(S,Se)_2$ solar cells by spray deposition of metal chalcogenides. *ACS Appl. Mater. Interfaces* 8, 11893-11897
69. Zhao, D. *et al.* (2016) Eliminating fine-grained layers in Cu(In,Ga)$(S,Se)_2$ thin films for solution-processed high efficiency solar cells. *J. Mater. Chem. A* 4, 13476
70. Deshmukh, S. D. *et al.* (2020) Investigating the potential of amine-thiol solvent system for high efficiency $CuInSe_2$ device. *2020 47th IEEE Photovoltaic Specialists Conference (PVSC)*, 0818-0820
71. Webber, D. H. *et al.* (2014) Facile dissolution of selenium and tellurium in a thiol-amine solvent system under ambient conditions. *Chem. Sci.* 5, 2498

72. Dolzhnikov, D. S. *et al.* (2015) Composition-matched molecular "solders" for semiconductors. *Science* 347, 425
73. Hudson, M. H. *et al.* (2017) New Forms of CdSe: molecular wires, gels, and ordered mesoporous assemblies. *J. Am. Chem. Soc.* 139, 3368−3377
74. Kovalenko, M. V. *et al.* (2010) Colloidal nanocrystals with molecular metal chalcogenide surface ligands. *Science* 324, 1417-1420
75. Buckley, J. J. *et al.* (2016) Dissolution of Sn, SnO, and SnS in a thiol-amine solvent mixture: insights into the identity of the molecular solutes for solution-processed SnS. *Inorg. Chem.* 55, 3175-3180
76. Davies, A. G. *et al.* (1988) The structures of 2,2-diakyl-1,3,2-dithiastannolanes. *J. Organomet. Chem.* 352, 283-294
77. Casella, G. *et al.* (2009) Karplus-type dependence of vicinal ^{119}Sn-^{13}C and ^{119}Sn-^{1}H spin-spin couplings in organotin(IV) derivatives: a DFT study. *Eur. J. Org. Chem.* 2009, 3526-3534
78. Wang, L. *et al.* (2015) Structure vs ^{119}Sn NMR chemical shift in three-coordinated tin(II) complexes: experimental data and predictive DFT computations. *Organometallics* 34, 2139-2150
79. Liu, S. *et al.* (2017) Lanthanide(III) complexes with μ-$SnSe_4$ and μ-Sn_2Se_6 linkers: solvothermal syntheses and properties of new Ln(III) selenidostannates decorated with linear polyamine. *Z. Naturforsch. B* 72, 231-240
80. Hsu, W.-C. *et al.* (2012) Reaction pathways for the formation of $Cu_2ZnSn(Se,S)_4$ absorber materials from liquid-phase hydrazine-based precursor inks. *Energy Environ. Sci.* 5, 8564-8571
81. Pirani, A. M. *et al.* (2001) Syntheses, vibrational spectra, and theoretical studies of the adamantanoid $Sn_4Ch_{10}^{4-}$ (Ch=Se, Te) anions: X-ray crystal structures of [18-Crown-6-K]$_4$[Sn_4Se_{10}]·5en and [18-Crown-6-K]$_4$[Sn_4Te_{10}]·3en·2THF. *Inorg. Chem.* 40, 4823-4829

Figure captions

Key figure

Periodic table of elements and their counterparts soluble in alkahest solutions

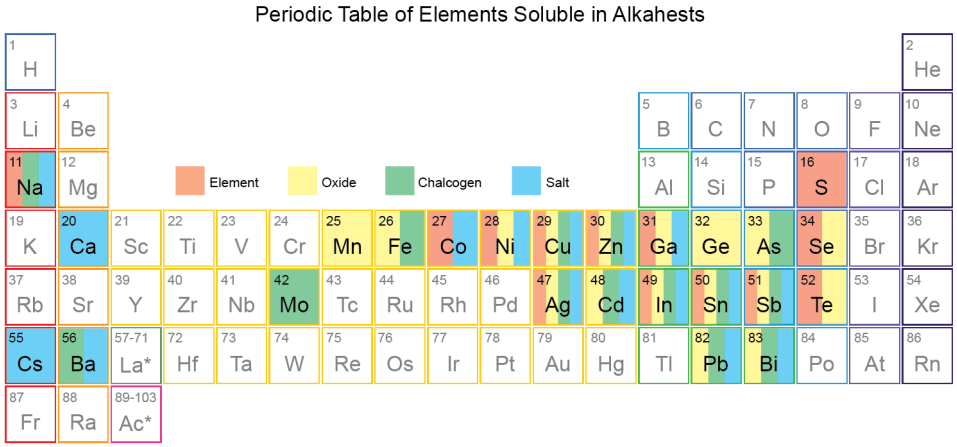

Figure 1. A comprehensive list of the types of soluble bulk precursors in alkahest solutions.

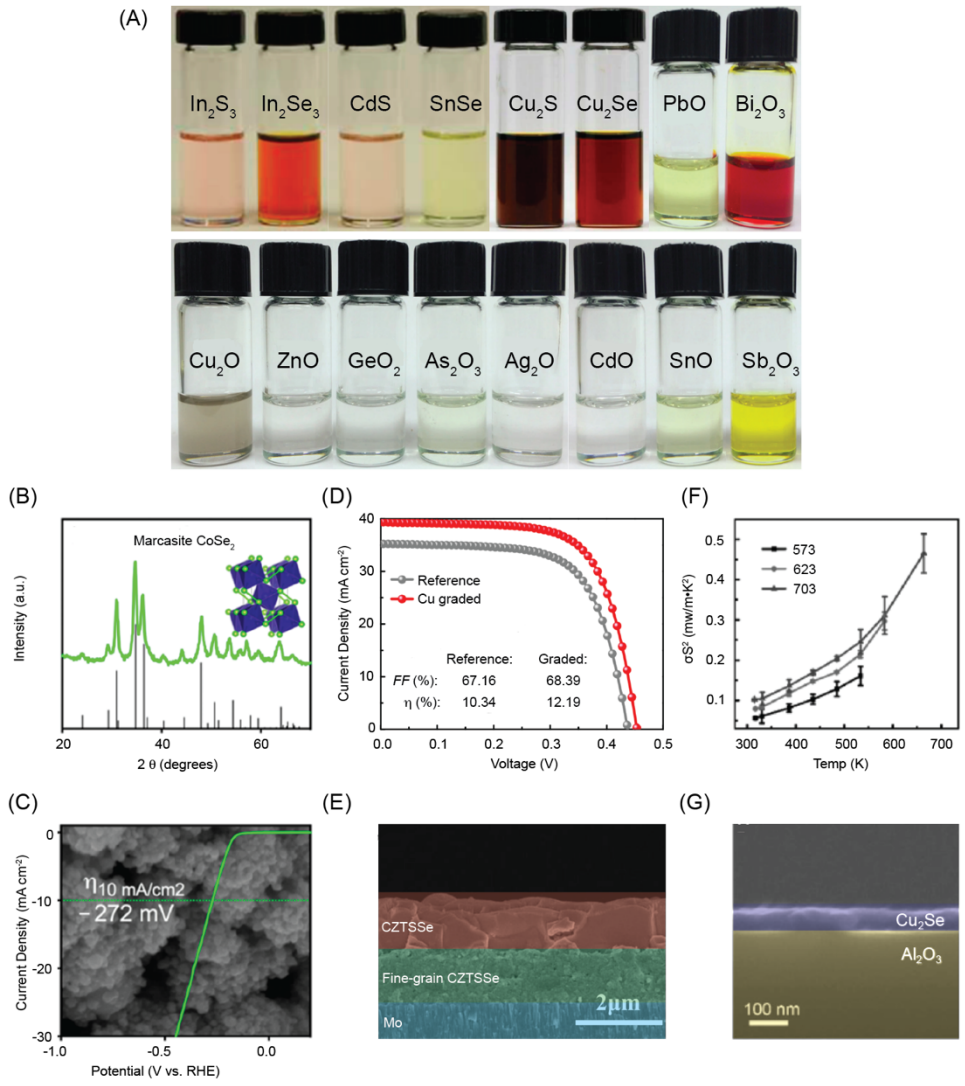

Figure 2. Applications of the alkahest. (A) Examples of various bulk solids dissolved in thiol-amine mixtures. (B) Powder X-ray diffraction pattern of solution-processed $CoSe_2$ from the dissolution of bulk Co and Se in ME–en with a representative marcasite crystal structure shown as the inset. (C) Polarization curve of a $CoSe_2$ thin film overlayed on top of an SEM image of solution-deposited $CoSe_2$. (D) *J-V* curves of bilayer structured Cu-poor and Cu-graded CZTSSe solar cells. (E) Cross-section SEM image of a Cu-graded CZTSSe solar cell with a bilayer absorber structure. (F) Power factor (σS^2) of Cu_2Se thin films deposited on polyimide substrates at different temperatures. (G) Cross-sectional SEM image of Cu_2Se deposited on an Al_2O_3 substrate. Adapted, with permission from, [12,22,25-27].

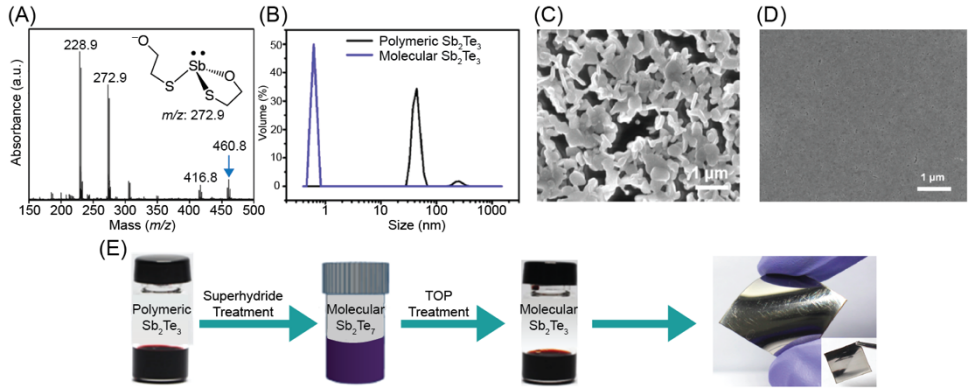

Figure 3. Bulk metal chalcogenide dissolution. (A) Negative ion mode ESI-MS of Sb_2S_3 dissolved in ME–en (1:40 vol/vol) with the structure of the molecular stibanate found at *m/z* = 272.9 shown as the inset. (B) DLS pattern of polymeric and molecular Sb_2Te_3 solutions. SEM images of thin films derived from (C) polymeric Sb-Te and (D) molecular Sb_2Te_3 precursors. (E) Schematic illustration of the procedure to produce molecular telluroantimonate precursors for thin film deposition on flexible polyimide substrates. Adapted, with permission from [38,42].

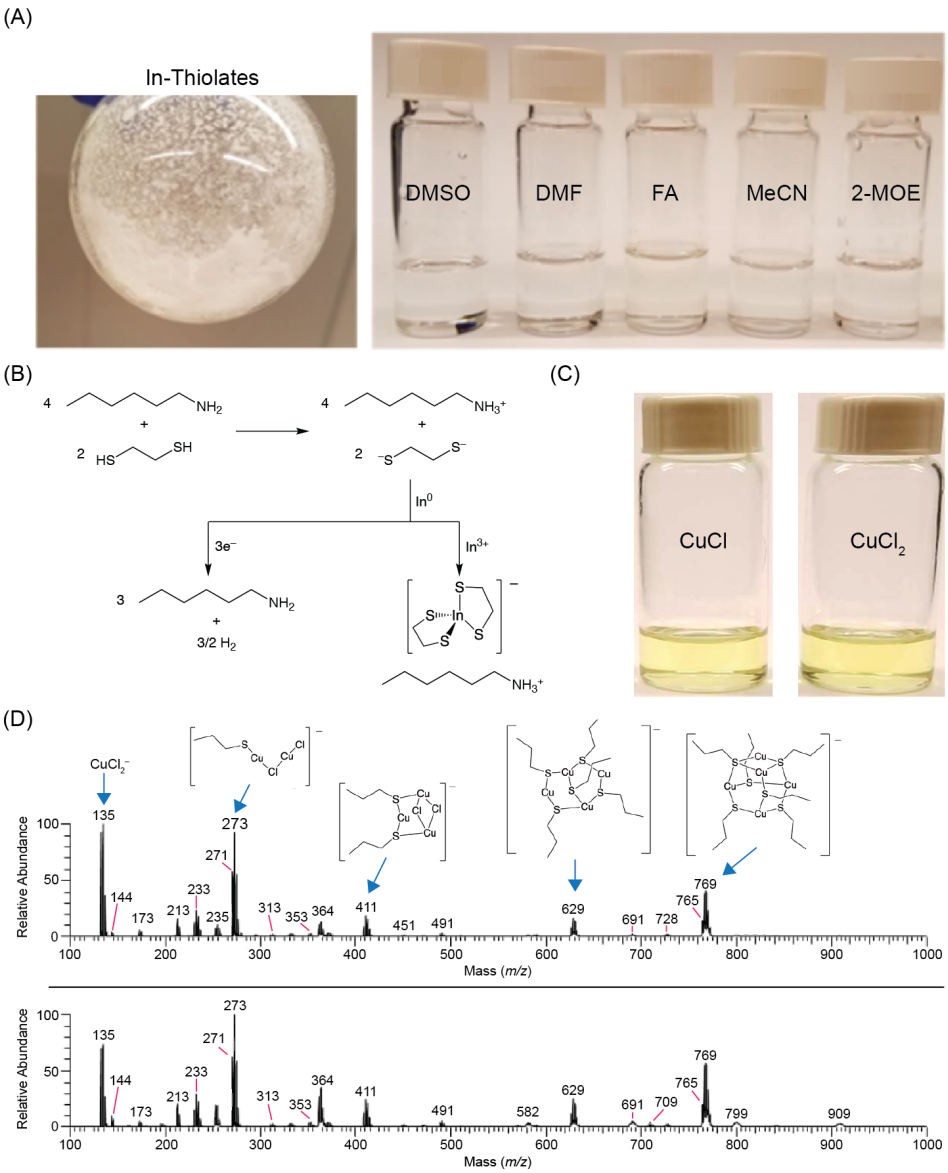

Figure 4. Bulk metal and metal salt dissolution. (A) Photographs of In-thiolates isolated and dissolved in various organic solvents (DMSO, DMF, FA, MeCN, and 2-methoxyethanol (2-MOE)). (B) Proposed dissolution pathway for In metal in dithiol-monoamine solutions. (D) Photographs of CuCl and $CuCl_2$ dissolved in a PT–BA solution. (D) Negative ion mode ESI-MS analysis of CuCl (top) and $CuCl_2$ (bottom) dissolved in PT–BA (1:1 mol/mol) solutions. Adapted, with permission from [18,62].

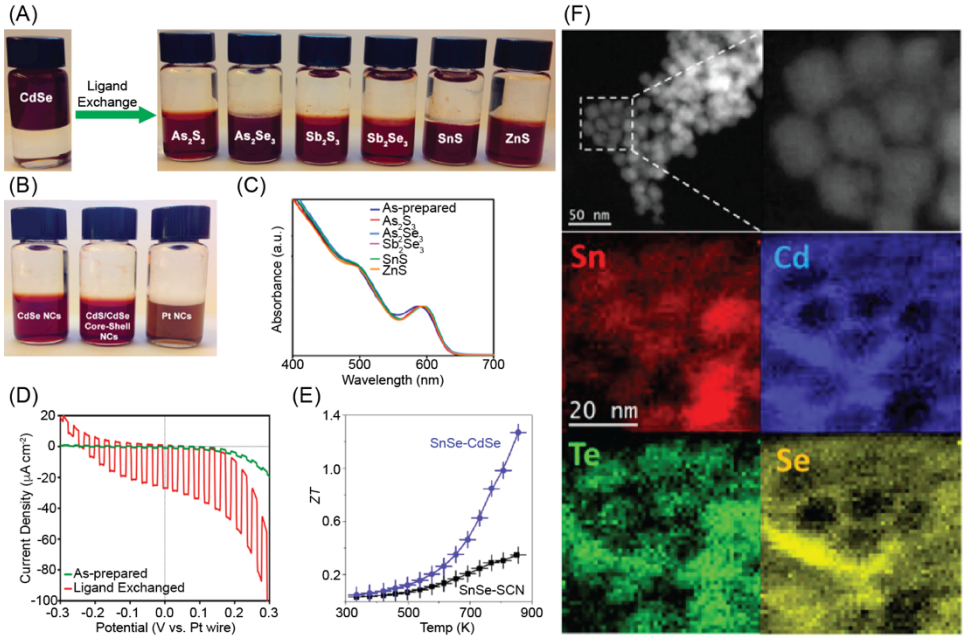

Figure 5. New applications of the alkahest. (A) Generality of the approach of installing dissolved bulk semiconductors onto the surface of CdSe nanocrystals. (B) Stibanate ligands installed on CdSe nanocrystals, CdS/CdSe core/shell nanocrystals, and Pt nanocrystals. (C) Solution absorption spectra of CdSe nanocrystals before and after ligand exchange with dissolved semiconductors. (D) Photocurrent response for ligand-exchanged CdSe nanocrystal films heat treated to 300 °C and as-prepared CdSe films heat treated to 150 °C during a potential scan from -300 to +300 mV relative to a Pt pseudoreference electrode with chopped 472 nm illumination. (E) Figure of merit (*ZT*) for SnTe nanocomposite prepared with thiocyanate (black) and CdSe (blue) surface modified SnTe nanocrystals. (F) Annular dark field (ADF) scanning transmission electron microscopy (STEM) micrograph of SnTe@CdSe nanocrystals and the corresponding STEM electron energy loss spectroscopy (EELS) elemental composition maps: Sn (red), Te (green), Cd (blue), and Se (yellow). Adapted, with permission from [38,40].

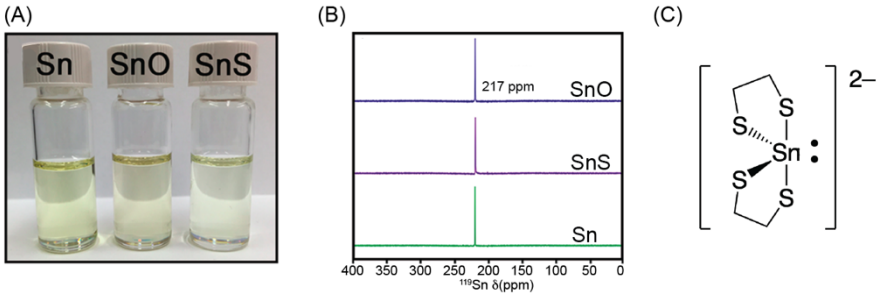

Figure I. Bulk Sn, SnO, SnS dissolution. (A) Photographs of bulk zero-valent Sn, SnO, and SnS dissolved in thiol-amine solutions. (B) Solution ^{119}Sn NMR spectra of Sn, SnO, and SnS dissolved in EDT−en giving a single resonance at δ_{119Sn} = 217 ppm. (C) Proposed structure of the $[(EDT)_2Sn(II)]^{2-}$ molecular solute from the dissolution of bulk elemental Sn, SnO and SnS in EDT–en. Adapted, with permission from [75].